Materials Advances

ROYAL SOCIETY OF CHEMISTRY

PAPER

View Article Online
View Journal | View Issue

Cite this: *Mater. Adv.*, 2025, 6, 7355

MiniSOG as a biodegradable heterogeneous photocatalyst for coupled redox biotransformations

Emmanouil Broumidis and Francesca Paradisi *

Received 6th August 2025,
Accepted 5th September 2025

DOI: 10.1039/d5ma00861a

rsc.li/materials-advances

Visible-light photocatalysis has emerged as a powerful strategy to drive chemical reactions under mild conditions, often in tandem with biocatalysts to achieve one-pot cascades. In this work, we demonstrate that the photocatalytic flavoprotein miniSOG, originally engineered as a genetically encoded singlet oxygen generator, can be repurposed as a heterogeneous photocatalyst. By immobilizing miniSOG as cross-linked enzyme aggregates (CLEAs), we enable controlled *in situ* production of hydrogen peroxide (H_2O_2) and NADH regeneration, facilitating both oxidative and reductive biotransformations.

Introduction

Heterogeneous photocatalysts offer significant advantages over homogeneous counterparts, such as simplified catalyst separation, improved catalyst recyclability, increased stability, and reduced environmental impact owing to their solid-state nature.[1–3] Recent studies have explored various heterogeneous photocatalysts, including titanium dioxide (TiO_2),[4] graphitic carbon nitride (g-C_3N_4),[5] conjugated porous polymers (CPPs),[6] and metal–organic frameworks (MOFs),[7] for applications such as water splitting,[8] pollutant degradation,[9] and organic synthesis.[10] Despite these advances, biodegradable heterogeneous (organic) photocatalysts have been relatively underexplored.

Recent research highlighted flavin-based photocatalysts as particularly promising due to their versatility and biocompatibility.[11] In particular, flavin mononucleotide (FMN) stands out among organic photocatalysts because its oxidised form absorbs strongly at ≈450 nm and, upon blue-light excitation, funnels efficiently to a long-lived triplet that is both a potent oxidant ($E^*_{red} \approx +2$ V *vs.* NHE) and—after single-electron reduction—a potent reductant ($FMN_{sq}/FMNH^{\bullet} \approx -1.1$ V). This bimodal redox behaviour lets FMN toggle between one- and two-electron pathways in neat water, providing a metal-free, recyclable alternative to Ru/Ir complexes;[12] by replacing the N5 atom with carbon (deazaflavins, dFl) and harvesting a second photon, chemists have pushed the excited-state potential beyond that of lithium metal [$E(dFl^*/dFl^{\bullet -}) = -3.3$ V *vs.* SCE] while retaining the parent cofactor's green credentials.[13] That versatility translates into a surprisingly broad reaction portfolio: free FMN mediates aerobic C–H oxygenation of alkyl benzenes on oxide supports,[14] drives visible-light [2+2] cycloadditions when tailored for energy-transfer catalysis,[15] and, in its super-reducing deazaflavin form, cleanly dechlorinates electron-rich arenes under air.[13] Additionally, FMN's ability to generate reactive oxygen species (ROS) upon light activation has been exploited in environmental applications, such as the degradation of micropollutants in water treatment processes.[16,17] Strategies for heterogenisation of flavins like embedding FMN within porous organic polymers,[17] inorganic particles (SiO_2,[16] ZrO_2/TiO_2[14]) or co-immobilization of free FMN and enzymes onto porous materials,[18] have been developed to enhance its photostability, ensuring prolonged catalytic activity, even in chemoenzymatic systems.

Beyond small-molecule catalysis, FMN's role as a natural cofactor in flavoproteins has been harnessed in photoenzymatic reactions. Enzymes such as old yellow enzymes (OYEs) utilize FMN to achieve stereoselective transformations under light irradiation, expanding the toolkit for asymmetric synthesis.[19,20] Particularly interesting is the miniSOG; a small, 106 residue (14 kDa) FMN-containing protein initially designed for singlet oxygen generation in correlative light and electron microscopy.[21] miniSOG has been shown to undergo both one- and two-electron reductions, demonstrating potential for diverse catalytic reactions.[22] Engineered miniSOGs, such as the Q103V variant, have been reported to enhance photocatalytic performance by extending the lifetime of its triplet excited state, enabling effective photoreduction reactions involving metal complexes such as Pt(IV) substrates.[23] Notwithstanding these very recent developments, miniSOG still remains primarily an imaging tool for microbiological applications, with a limited scope in its use as a photocatalyst.[24]

Department of Chemistry, Biochemistry and Pharmaceutical Sciences, University of Bern, Bern 3012, Switzerland. E-mail: francesca.paradisi@unibe.ch

By leveraging the inherent biodegradability and the versatile photocatalytic capabilities of FMN, we envisioned that utilizing miniSOG's scaffold for heterogenization of the chromophore could significantly enhance its practical applicability, stability, and recyclability, thereby addressing critical limitations of homogeneous systems.

Results and discussion

Preparation of miniSOG WT and Q103V mutant

The proteins were prepared in house as previously reported (see Fig. S1 and S2), achieving a yield of ~30 mg L^{-1} of purified protein, in line with literature reported values.[25]

Singlet oxygen generation

To evaluate whether miniSOG can deliver synthetically useful fluxes of singlet oxygen ($^1O_2$) in solution, we first carried out photooxygenations under homogeneous conditions. Classical $^1O_2$ reporters were chosen (Scheme 1): (i) α-terpinene, whose conversion to ascaridole can be followed by ^1H NMR,[26] and (ii) triphenylphosphine (PPh_3), which oxidises to triphenylphosphine oxide and can be monitored by ^{31}P NMR.[27] Reactions were performed in $CDCl_3$ containing 10% v/v D_2O potassium phosphate (KPi) buffer (pD 7.4, 50 mM) to extend the lifetime (τ_Δ) of $^1O_2$, which is 20–25-fold longer in D_2O than in H_2O.[28,29] A fully aqueous test with the water-soluble substrate 2-furoic acid, a recognised benchmark for $^1O_2$ oxidation, was run in parallel (iii).[30] Even under conditions designed to maximise $^1O_2$ yield (0 °C, deuterated solvents, O_2-sparging, 450 nm LEDs, miniSOG = 5 mg mL^{-1}) no ascaridole, triphenylphosphine oxide or 5-hydroxy-2(5*H*)-furanone could be detected within the NMR limits of quantification. This outcome is consistent with the low solution quantum yields reported for native miniSOG ($\Phi_\Delta \approx 0.03$–0.06)[31] and with structural studies showing efficient quenching of its FMN triplet by the surrounding protein matrix.[25] Although engineered variants and cellular contexts can enhance phototoxicity,[32,33] our results indicate that unmodified miniSOG is ill-suited for preparative $^1O_2$ chemistry in homogeneous solution without further protein or cofactor optimisation.

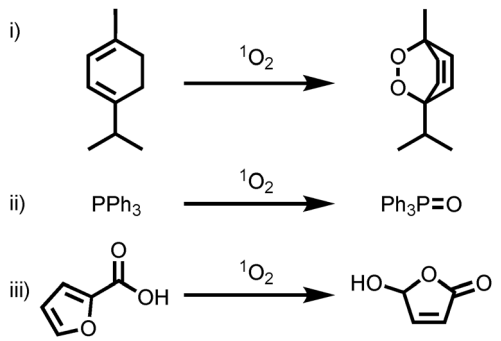

Scheme 1 Attempts at use of miniSOG for photoinduced singlet oxygen generation.

Hydrogen peroxide and speroxide radical production

We then redirected our efforts to type-I electron-transfer photochemistry (PS* to $^3O_2$, producing ROS), specifically the light-driven formation of hydrogen peroxide (H_2O_2). A continuous, micromolar-scale flux of *in situ* H_2O_2 is especially valuable for biocatalysis, because many peroxide-dependent enzymes (*e.g.*, heme-thiolate peroxygenases) suffer rapid, irreversible heme degradation when exposed to the millimolar peroxide boluses typically added from a syringe, yet remain active if H_2O_2 is fed slowly and uniformly.[34] We previously reported on the efficiency and stability of a photobiocatalytic flow system which could deliver brominations *via* an internally generated, steady trickle of peroxide.[35] Similar "self-dosing" strategies have proved crucial for unspecific peroxygenase cascades in which photocatalysts, including flavin photosensitisers furnish only as much H_2O_2 as the enzyme can safely consume.[36–38]

For the heterogenization of miniSOG, covalent attachment of wild-type (WT) miniSOG to commercial epoxy- and amino-activated beads was explored first, yet the preparations lost fluorescence and activity quickly under irradiation (see Fig. S3 and S4). The Q103V mutant, whose triplet lifetime (~100 μs) indeed boosts H_2O_2 output in solution as previously reported, proved equally impractical: the FMN cofactor detached during metal-affinity chromatography and again when the protein solution was reduced to achieve a concentration of ~5 mg mL^{-1} for downstream experiments, suggesting a weakened chromophore interaction.

The weakened binding most likely arises because Gln103 promotes FMNs stability *via* H-bonding (Fig. 1(c)); its replacement with hydrophobic residues such as valine or leucine eliminates the non-covalent interaction, a drawback noted previously for Q103V/L in other contexts.[39,40]

These setbacks steered us toward the cross-linked enzyme aggregate (CLEA) strategy, a carrier-free immobilisation concept in which the target enzyme is (i) precipitated from a concentrated solution so that the molecules cluster into nano-

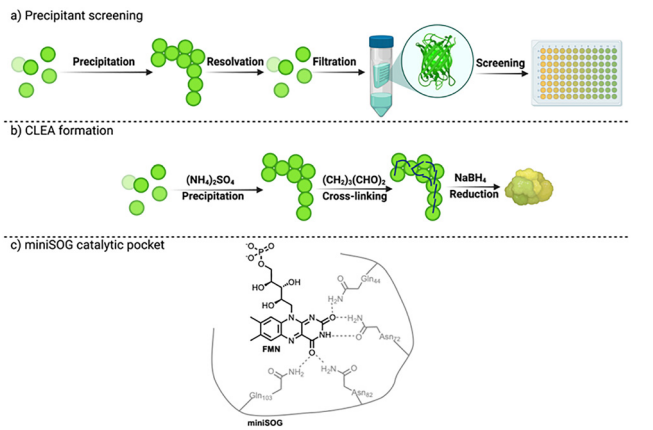

Fig. 1 CLEA preparation workflow that included (a) determination of ideal precipitating agent and (b) glutaraldehyde (cross-linking) percentage (second step). See Fig. S7. (c) Catalytic pocket of miniSOG, containing the FMN chromophore.

to micrometre aggregates, and (ii) the resulting protein clusters are covalently ''locked'' with a bifunctional reagent such as glutaraldehyde, which forms Schiff-base bridges between surface lysines.[41]

Immobilising miniSOG as CLEAs would offer a carrier-free, recyclable and biodegradable photocatalyst format that tightly entraps the flavin in the protein matrix, while enabling straightforward recovery.[42] Despite the fact that CLEAs have been prepared for a variety of biocatalysts, no reports on the efficiency of this strategy for small proteins like miniSOG has been published to date. In particular, structural distortion (with potential loss of the FMN) or minimal efficiency of the cross-linking could be encountered due to the distribution of the six surface lysine residues in miniSOG (SI, Fig. S5). We started our CLEA optimization campaign with two critical parameters, precipitant selection, and cross-linker amount (Fig. 1(a) and (b)).

Precipitant selection

CLEA preparation begins with the precipitation of folded protein (as opposed to inducing unfolding which would also results in protein precipitation). Because miniSOG lacks a routine activity assay, we monitored denaturation indirectly: precipitation (200 μL, 5 mg mL^{-1}) was induced with 12 candidate agents at ≈90% of their customary concentration; after 5 min, precipitates were redissolved by adding 1800 μL of buffer (100 mM KPi pH 7.0) solution, centrifuged through a 10 kDa filter, and FMN fluorescence in the filtrate (λ_{ex} 450 nm/λ_{em} 520 nm) quantified. Loss of FMN correlates with unfolding. Ammonium sulfate $(NH_4)_2SO_4$—long regarded as the gentlest salting-out agent for enzymes[43]—released virtually no FMN (≲baseline), whereas 1-propanol liberated ≈90% of the chromophore, making it the worst choice (Fig. 2(a)). PEG-400, methanol and ethanol displayed intermediate effects. Thus, ammonium sulfate (90% sat.) was adopted for all subsequent CLEA preparations.

Reaction-medium engineering

Having established that 90%-saturated ammonium sulfate cleanly precipitates holo-miniSOG without ejecting FMN, our next priority was to tailor the reaction environment in which these CLEAs operate. The composition of this reaction medium governs the photoredox fate of the trapped flavin—especially its propensity, under blue light, to divert electrons toward oxygen and form superoxide. Triethanolamine (TEOA), a tertiary amine commonly used in photocatalytic cycles,[44] boosted H_2O_2 production from 1.4 μM (KPi only) to 10 μM at 10 mM, but fell to 6 μM at 100 mM—consistent with donor-excess quenching of excited FMN (Fig. 2(b)). Because superoxide dismutase (SOD) catalyses $O_2^{\bullet-} \rightarrow H_2O_2 + O_2$ near the diffusion limit ($\sim 2 \times 10^9$ M^{-1} s^{-1}),[45] adding 1 U SOD in the system doubled the H_2O_2 yield to ≈23 μM, confirming superoxide as the primary ROS intermediate. These observations are in agreement with classical FMN photochemistry, where reduced flavins (by an electron donor, like EDTA or TEOA) react with O_2 to form H_2O_2 *via* superoxide.[46] Moreover, it has been proven that miniSOG not only generates $O_2^{\bullet-}$, but it's actually one of the primary ROS that it produces, and, is able to diffuse out of the protein structure into the surrounding medium.[47,48]

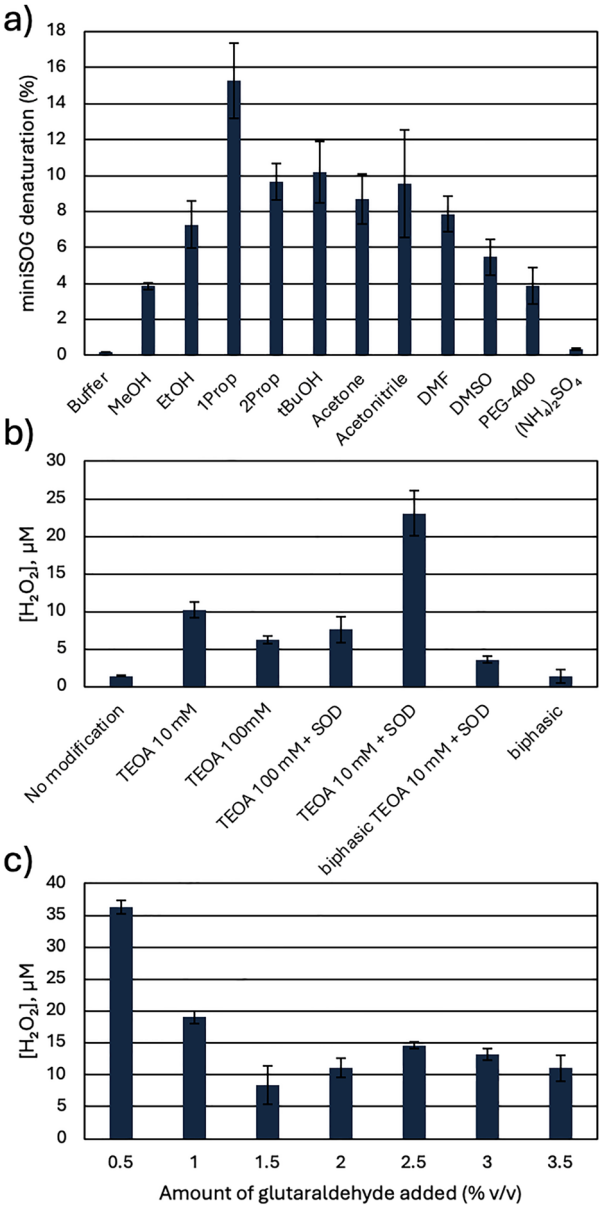

Fig. 2 (a) Precipitant screen. (b) Reaction additive screen. (c) Glutaraldehyde dose optimisation. All data represent mean ± SD (n = 3). H_2O_2 quantification determined by HRP/ABTS assay using a calibration curve (Fig. S6).

Cross-linker optimisation

Aggregates were stabilised with glutaraldehyde (GA), the most widely used bifunctional cross-linker in CLEA technology owing to its low cost and broad reactivity with lysine ε-amines.[49] Yet excessive GA can rigidify the protein matrix and throttle mass transfer, while too little fails to lock particles together.[50] We therefore varied GA between 0.5 and 3.5% v/v. Photocatalytic assays (Fig. 2(c)) revealed a clear optimum at 0.5% GA, giving 100% relative H_2O_2 output; higher loadings depressed

activity, in line with literature reports that over-cross-linking introduces diffusional barriers,[51] while concentrations below 0.5% v/v did not lead to appreciable CLEA formation. It is also noted that after crosslinking, the $NaBH_4$ reduction step is crucial, as without it, the CLEAs degrade due to hydrolysis of the imine bonds formed between glutaraldehyde and lysine residues, and the FMN chromophore remains inactive. Consequently, the unreduced, deep-orange material does not generate detectable H_2O_2 upon irradiation. Once reduced, the finalised CLEA can be lyophilised and stored at −20 °C for at least one month without loss of ROS-producing ability.

Characterization of miniSOG CLEAs

To confirm successful CLEA formation and understand their structural features, we characterized the aggregates using Fourier transform infrared spectroscopy (FT-IR), dynamic light scattering (DLS), and scanning electron microscopy (SEM) (Fig. 3). IR spectra of the CLEA (orange trace) compared to the pre-crosslinked precipitate (blue trace) revealed a persistent amide I band at ~1650 cm^{-1} and amide II at ~1540 cm^{-1}, suggesting successful retention of protein secondary structure in the CLEA material.[52] Furthermore, significant increases in aliphatic C–H signals (*e.g.* 2925–2850 cm^{-1}) from glutaraldehyde's methylene groups, confirm that the protein molecules are covalently interconnected *via* glutaraldehyde. These features match typical CLEA spectral fingerprints reported previously.[53,54]

DLS analysis of suspended CLEAs revealed a broad particle size distribution centred between 5–8 μm, far larger than the native enzyme, indicating aggregation of many protein units into each CLEA particle.

Such large sizes are common in CLEA preparations without dispersants or co-feeders, where inter-protein crosslinking leads to extensive agglomeration.[53,55]

SEM micrographs further confirmed the aggregated morphology: the CLEAs appeared as rough, porous clusters composed of smaller, 4–8 μm subunits (Fig. 3(c) and (d)), in

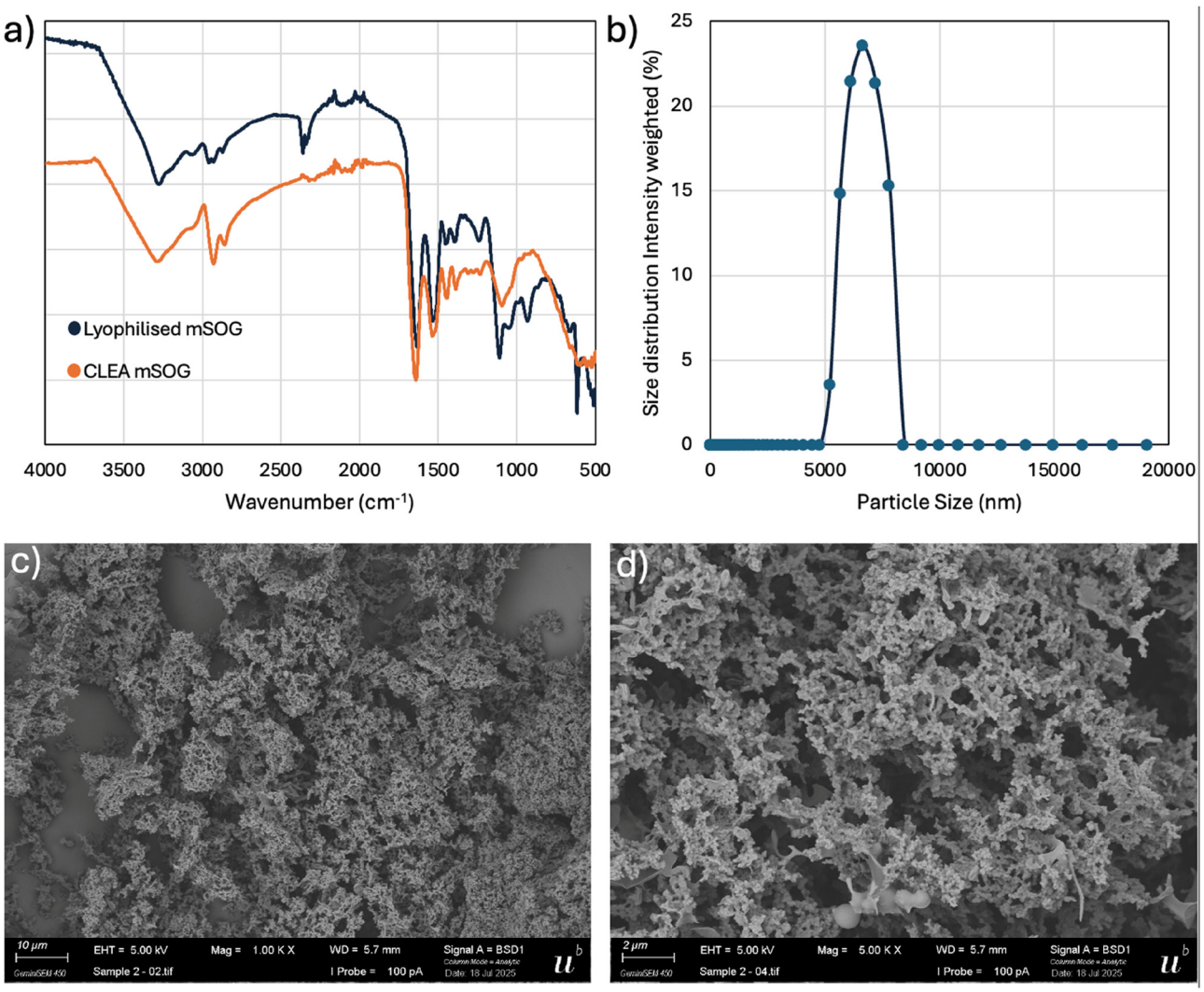

Fig. 3 Physicochemical characterisation of miniSOG CLEAs. (a) FTIR spectra of precipitated miniSOG (blue) and cross-linked aggregates (orange). (b) DLS size distribution showing aggregated particles (5–8 μm). (c), (d) SEM micrographs revealing type I/II porous, spherical aggregates typical of protein CLEAs. Scale bars: (c) 10 μm, (d) 2 μm.

agreement with the DLS observations. According to the classification by Sheldon *et al.*,[56] these can be classified as composite type I/type II CLEAs, with spherical subunits partially fused into irregular, porous aggregates.

Together, the spectroscopic, hydrodynamic, and morphological evidence confirms successful conversion of miniSOG into a covalently crosslinked, insoluble aggregate.

Evaluation of the system

Having established the conditions in which the miniSOG-CLEA/TEOA/SOD gave the most constant sub-millimolar H_2O_2 flux (Fig. 2(b)), we explored whether the peroxide stream is compatible with a peroxide-sensitive heme enzyme—an unspecific peroxygenase (UPO)—and could drive a synthetically useful oxyfunctionalisation (Fig. 4(a)). As model substrate we chose 1*H*-indole-7-carboxylic acid (1 mM), whose carboxylate renders the indole core water-soluble, avoiding the mass-transfer limits that affect the parent indole.[57] Recombinant AaeUPO (10 μM; heme-thiolate active site) was combined with 5 mg miniSOG-CLEA in 100 mM KPi (pH 7.0) containing 10 mM TEOA and 1 U SOD; the suspension (1 mL, 2 mL Eppendorf) was irradiated for 30 min with 450 nm (10 W, orbital shake 100 rpm) and then analysed.

LC–MS revealed ~82% conversion of the indole after a single 30-min light period (Fig. 4(b) and Fig. S8), and ~80% of the product peak corresponded to the expected 3-oxindole (*m*/*z* 177.0 $[M + H]^+$, Fig. S9), the most common monooxygenation product for UPO-catalysed indole oxidations.[58] Minor signals for dimeric or over-oxidised species—crosslinked indoles routinely observed in UPO chemistry—were also detected. By contrast, dark controls (no *hν*) or reactions lacking the CLEA photocatalyst or the UPO protein gave ≤3% conversion, confirming that *in situ* peroxide formation is mandatory (Fig. S10). Furthermore, the regioisomer of **1**, 1*H*-indole-6-carboxylic acid was also employed under otherwise identical conditions, and the same outcome was observed; after 1 h of irradiation, 100% conversion was achieved (Fig. S11).

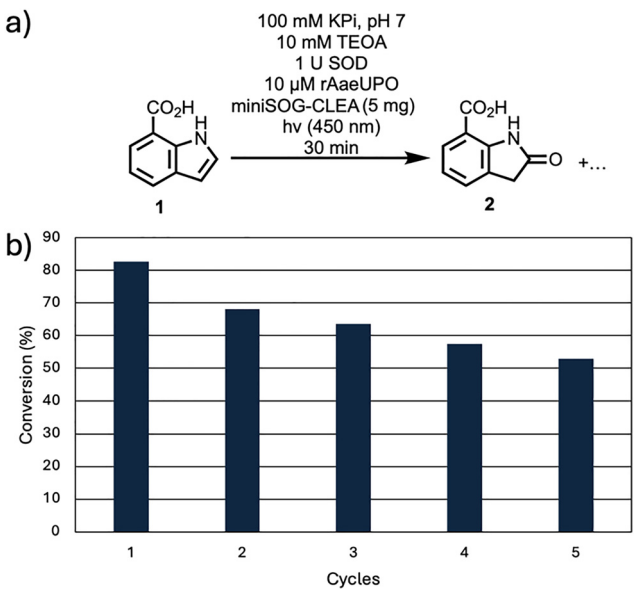

Fig. 4 (a) Reaction scheme and conditions for the blue-light mediated oxidation of **1** (1 mM) to oxindole **2** using rAaeUPO and *in situ* produced H_2O_2 from miniSOG-CLEA. (b) Recyclability test of the miniSOG-CLEA photocatalyst.

Re-usability

After the reaction was complete the reaction mixture was centrifuged, washed and the miniSOG-CLEA pellet was resuspended by addition of 1 mL of fresh reaction mixture for four further 30-min cycles (identical conditions, Fig. 4(b)). Conversion declined gradually from ~82% (cycle 1) to ~52% (cycle 5), reflecting progressive but not catastrophic FMN bleaching (as opposed to leaching); miniSOG is known to inactivate under prolonged exposed to excess light *via* ROS promoted chromophore destruction,[25,59] yet the CLEA material clearly tolerates this effect. HPLC analyses of the clear supernatant after each reaction showed only minor traces of leached FMN chromophore, confirming that photobleaching is the main avenue for catalyst degradation over time.

These observations demonstrate that the miniSOG-CLEA platform supplies a UPO-compatible, self-metered H_2O_2 flux, enabling the successful oxidation of carboxy-indoles and providing a proof-of-concept for coupling miniSOG-CLEAs with other peroxide-sensitive oxidations.

Oxidative system benchmarking

To benchmark the oxidative performance of miniSOG-CLEA we compared its apparent quantum yield Φ_{app} and photocatalyst-normalised turnover frequency TOF with two representative heterogeneous photocatalysts previously reported for visible-light-driven UPO reactions (Table 1). MiniSOG-CLEA not only gives the highest peroxide productivity per gram of catalyst (Table 1, entry 1), but also exhibits the best photon economy in the set outperforming Au-decorated TiO_2 nanoparticles (NP) (Table 1, entry 2) and melon-type g-C_3N_4 (Table 1, entry 3). These results show that a biodegradable protein scaffold can already match or surpass state-of-the-art inorganic supports, while leaving room for further improvement through chromophore engineering or light-management strategies.

NADH recycling

Beyond their utility as recyclable H_2O_2 photo-generators, we reasoned that miniSOG-CLEAs might also function as photocatalysts for NADH regeneration, an ever-present bottleneck in nicotinamide-dependent biocatalysis.[60] Our interest was sparked by a 2019 report from Kinastowska *et al.* showing that, under strongly alkaline conditions (pH ≥ 10) and high triethanolamine (TEOA) loadings (0.5–1 M), a range of heterogeneous photosensitisers photo-oxidise TEOA to glycolaldehyde (GlyA); GlyA then reduces NAD^+ to enzymatically active 1,4-NADH even after the photocatalyst is removed and the lights are off.[61]

TEOA thus could serve the dual role of sacrificial electron donor and a precursor of the GlyA reductant. To verify that miniSOG-CLEAs indeed photo-generate the glycolaldehyde required for nicotinamide reduction, we quantified GlyA production

Table 1 Visible-light heterogeneous H_2O_2 generators for peroxygenase reactions[a]

Entry	PS	Light source/time (h)	H_2O_2 (μmol)	Φ_{app} (%)	TOF (μmol g^{-1} h^{-1})
1	MiniSOG-CLEA (this work)	10 W LED strip, 0.5 h	0.82	0.0012	330
2	Au–TiO_2 NPs	150 W halogen, 6 h	0.96	0.0011	32
3	g-C_3N_4 powder	205 W halogen, 1 h	0.12	0.00028	24

[a] Detailed calculations for deriving Φ_{app} and TOF values can be found in SI, Page S27.

by repeating the trapping protocol of Yuehui *et al.*,[62] which consists in reacting GlyA with 3-methyl-2-benzothiazolinone hydrazone (MBTH) to generate its oxime–hydrazone adduct (MBTH-GlyA) for subsequent UV and mass detection by LC–MS (Fig. 5(a) and Fig. S12–S14). Under our adapted conditions (0.5 M TEOA, NH_3/NH_4^+ buffer, pH 10.5, 30 min irradiation) the CLEA suspension produced ≈1.8 mM GlyA (Fig. 5(b)), consistent with the 3–5 mM range reported for semiconductor photocatalysts.[61] Moreover, ^{1}H-NMR analysis of the illuminated reaction mixture (Fig. 5(b), D_2O, 0.5 M TEOA, pD 10.5) revealed the clear appearance of glycolaldehyde-specific resonance, a singlet at δ 9.56 ppm (1 H, –CHO), identical to a GlyA standard. These signals are absent in both the dark control and the "no-CLEA" control, confirming that they originate from the photo-induced oxidation of TEOA mediated by miniSOG-CLEA.

An additional experiment confirmed that, after 30 min irradiation of miniSOG-CLEAs at pH 10.5, the cleared reaction supernatant reduced NAD^+ to ~40% NADH within 1 h in the dark (Fig. 5(c)). These results corroborate that FMN is indeed capable of acting as a photocatalyst for the production of GlyA.

Because this highly alkaline medium (optimal GlyA formation is recorded at pH ≈ 11.5) is too extreme for most redox enzymes, we sought a compromise that still supports appreciable GlyA formation yet allows enzymatic turnover. Phenylalanine dehydrogenase (PheDH) is an attractive test case: it catalyses the NADH-dependent reductive amination of phenylpyruvate in NH_3/NH_4^+ buffer (ammonia source) at an optimum pH of 9.5, while retaining more than half of its activity at pH 10.5.[63,64] Adopting pH 10.5 in a TEOA/NH_3 system therefore (i) keeps GlyA production within one order of magnitude of its optimum and (ii) places PheDH within its activity tolerance threshold, enabling the photogenerated GlyA to reduce NAD^+ *in situ* and drive PheDH turnover (Fig. S15).

When PheDH (7 U mL^{-1}, as measured in these optimised conditions) and phenyl-pyruvate (**3**) (2 mM) were added and illuminated (450 nm light), > 60% of the starting material **3** was consumed to form L-phenylalanine within 30 min (Fig. 6(a)), demonstrating an operational photo-enzymatic NADH-recycling loop compatible with alkaline biocatalysts (Fig. S16). Upon blue

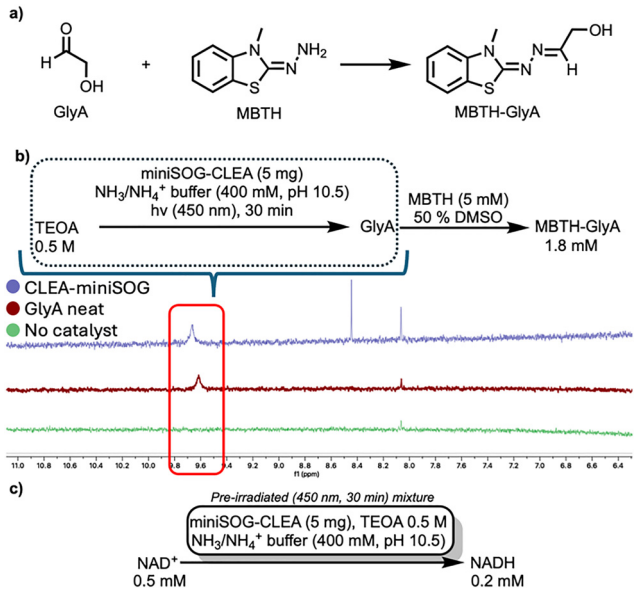

Fig. 5 Photochemical generation of glycolaldehyde (GlyA) and NADH using miniSOG-CLEA. (a) GlyA derivatisation with 3-methyl-2-benzothiazolinone hydrazone (MBTH) to give the UV-detectable adduct MBTH-GlyA 3. (b) GlyA formation: irradiation of miniSOG-CLEA (5 mg) in 0.5 M TEOA/400 mM NH_3/NH_4^+ buffer (pH 10.5) for 30 min (450 nm) affords 1.8 mM GlyA, quantified as MBTH-GlyA. No GlyA is detected in dark or "no-CLEA" controls. ^{1}H-NMR spectra of highlighted reaction products. Peak at ~8.5 can be attributed to miniSOG degradation. (c) The pre-irradiated mixture (pre-NAD^+ addition) reduces NAD^+ (0.5 mM) to enzymatically active NADH (0.2 mM) within 1 h in the dark, confirming GlyA-mediated cofactor regeneration.

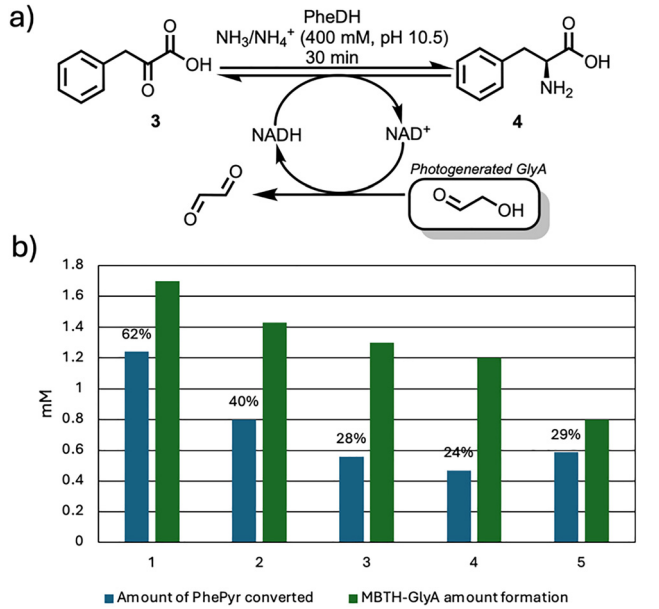

Fig. 6 Coupling photogenerated glycolaldehyde to PheDH-catalysed reductive amination. (a) Reaction scheme. (b) Recycling study (five 30-min irradiation cycles; 5 mg CLEA, 0.5 M TEOA, 0.2 mM NAD^+, in 1 mL). Blue bars: PhePyr converted (%) green bars: GlyA formed (mM, quantified as MBTH adduct). Product formation parallels GlyA availability. No product was detected in "no-light" or "no-CLEA" controls.

light illumination, the miniSOG-CLEA produces glycolaldehyde (GlyA), which reduces NAD^+ to NADH; the latter drives phenylalanine dehydrogenase (PheDH) to convert phenyl-pyruvate **3** (2 mM) into L-phenylalanine **4** in NH_3/NH_4^+ buffer (400 mM, pH 10.5, 30 min). In principle, the dialdehyde (glyoxal) that is formed after GlyA is oxidised can then be a NAD^+ reductant on its own. Furthermore, as with the oxidative system, we tested the durability of the photocatalyst under these alkaline conditions; in each recycling run we tracked both phenyl-pyruvate (PhePyr) conversion and the amount of glycolaldehyde (GlyA) trapped as its MBTH adduct (Fig. 6(b)). The two profiles correlate closely: GlyA is generated at 1.7 mM in the first light period and falls steadily to $\approx$0.8 mM by the fifth, mirroring the drop in PhePyr conversion from 62% to 29%. The slight rebound in cycle 5 (GlyA $\approx$0.8 mM; conversion 29%) reflects the experimental scatter but underscores that conversion is limited by the GlyA (and hence NADH) pool rather than PheDH itself, whose specific activity remains high at pH 10.5/NH_3 buffer. Control experiments confirmed that product formation requires all three components: (i) irradiated CLEA, (ii) TEOA and (iii) PheDH—no product was detected when light was omitted, or the atmosphere was replaced with N_2.

Finally, the used miniSOG-CLEA material was further characterised with FT-IR and SEM to determine its physicochemical condition after use. The former showed an identical spectrum, with the key amide I and II bands remaining present (Fig. S17). Furthermore, the SEM micrographs showed that the surface morphology remained unaltered after five consecutive reaction cycles (Fig. S18). This observation shows that the protein backbone of the material remains intact, and the inactivation of the catalyst is indeed attributed to the photobleaching of the FMN chromophore.

We also attempted a combi-CLEA in which PheDH was co-precipitated (Fig. S19) and cross-linked with miniSOG, following precedents for tandem CLEAs in oxidoreductase cascades.[65,66] Although the material formed readily, PheDH lost >95% activity after cross-linking, likely due to glutaraldehyde modification of its catalytic lysine, and no detectable product formed under illumination. These observations emphasise that a two-component set-up—photocatalytic miniSOG-CLEA plus freely diffusing PheDH—is currently the most effective arrangement for the GlyA/NADH relay.

To ensure that the low, steady-state H_2O_2 released by miniSOG-CLEA would not compromise the reductive amination step, we conducted a separate experiment using PheDH with a deliberately harsh peroxide load. The enzyme (7 U mL^{-1}, NH_3/NH_4^+ buffer, pH 10.5) was pre-incubated for 60 min with 1 mM H_2O_2—over twenty-fold higher than the $\approx$40 μM generated photochemically in each cycle—then assayed in the standard PhePyr → L-Phe reaction. Residual activity was indistinguishable from an untreated control (<3% difference, n = 3), indicating that PheDH tolerates peroxide levels well above those present during the coupled process. Consequently, the addition of catalase or other peroxide-scavenging enzymes, often required in flavin-driven NADH systems, was unnecessary in our set-up.

Taken together, the data demonstrate a clear stoichiometric link between photogenerated GlyA, NADH availability and product formation, and establish miniSOG-CLEA as a recyclable, carrier-free photocatalyst that can power NADH-dependent reductive biocatalysis under alkaline conditions.

Reductive system benchmarking

To situate miniSOG-CLEA within the broader NADH-photoregeneration landscape we assembled a concise comparison of apparent quantum yields (Φ_{app}) and catalyst-normalised initial rates (TOF) against three representative heterogeneous systems (Table 2). miniSOG-CLEA reaches $\Phi_{app} \approx 1 \times 10^{-5}$ (0.001%) and TOF $\approx$ 80 μmol g^{-1} h^{-1}, values near those of the conjugated organic polymer PHTT_DMP and bulk g-C_3N_4 reported by Kinastowska *et al.*[61] (Table 2, entries 2 and 3) and substantially lower than the engineered visible-light TiO_2@g-C_3N_4 core–shell catalyst of Dong Yang *et al.* (Table 2, entry 4).[67] Notwithstanding its modest photon economy, miniSOG-CLEA offers advantages unique to a biodegradable protein scaffold—straightforward genetic tuning, facile removal from product streams, and dual oxidative/reductive functionality—which collectively justify further optimisation efforts.

Mechanistic pathway

With these experiments we have now exploited both branches of the miniSOG (FMN) photoredox manifold (Scheme 2): (i) the reductive leg, in which the FMN triplet oxidises TEOA step-wise to glycolaldehyde (GlyA), and GlyA in turn delivers the two-electron hydride required to convert NAD^+ into enzymatically competent NADH, and, (ii) the oxidative leg, in which photoreduced $FMN^{\bullet -}$ transfers an electron to O_2 to give $O_2^{\bullet -}/H_2O_2$, fuelling haem peroxygenase catalysis. To our knowledge this is

Table 2 Benchmark comparison of four heterogeneous NADH-photoregeneration systems

Entry	PS	Illumination and time	Reactor volume/catalyst loading	NADH formed (μmol)	Φ_{app} (%)	TOF (μmol g^{-1} h^{-1})
1[a]	MiniSOG-CLEA (this work)	450 nm LED strip, 30 min	1 mL, 5 mg CLEA	0.20	0.001	80
2[a]	PHTT_DMP polymer[61]	400–700 nm lamp, 2 h	5 mL, 10 mg polymer	0.50	0.002–0.004	50
3[a]	g-C_3N_4[61]	400–700 nm lamp, 2 h	5 mL, 10 mg g-C_3N_4	0.50	0.002	50
4[b,c]	TiO_2@g-C_3N_4 core–shell[67]	405 nm LED, 1 h	4 mL, 5 mg composite	4.0	0.17	800

[a] Φ_{app} and TOF were calculated based on experimental values. Detailed calculations can be seen at SI, Page S30. [b] Φ_{app} value was provided directly by the authors of the study. [c] In addition to the composite catalyst, an electron mediator, $[Cp^*Rh(bpy)H_2O]^{2+}$, was also employed in order to facilitate electron transfer from TEOA to NAD^+.

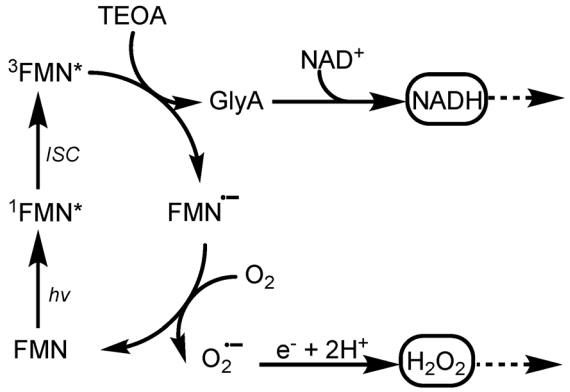

Scheme 2 Dual photoredox pathways of miniSOG's FMN: oxidative branch (O_2 → H_2O_2) and reductive branch (TEOA → GlyA → NADH). The TEOA → GlyA → NADH branch operates only under alkaline conditions (this work: 0.5 M TEOA in NH_3/NH_4^+ buffer, pH 10.5, 450 nm irradiation, 30 min). The oxidative branch (photo-reduced FMN → $O_2^{\bullet-}$/H_2O_2) is run in neutral phosphate buffer as described in the text.

the first demonstration that an FMN photosensitiser can drive GlyA formation from TEOA and propagate that chemistry into a functional NADH-recycling loop (photochemical GlyA → NADH → PheDH turnover). Conventional photobiocatalytic systems usually harness only one half-reaction, the oxidation of a ''sacrificial'' donor whose products are discarded, while the complementary reduction channel remains unused.

By coupling both directions we achieve dual functionality from a single, carrier-free miniSOG-CLEA catalyst: a controlled H_2O_2 source for oxidative enzymes and, under alkaline conditions, a renewable NADH generator for reductive biocatalysis. This dual exploitation of FMN photochemistry expands the toolbox of flavin-based photocatalysts and showcases a rare example where the oxidation products of the sacrificial donor are valorised rather than wasted.

Conclusions

This proof of concept showcases that miniSOG has the potential to be exploited as more than a mere cell deactivator/fluorescent tag for microbiology studies and expand its application scope into the realm of synthetic chemistry. We were able to successfully use miniSOG in conjunction with other proteins (UPO, SOD, PheDH), further highlighting its compatibility with protein cascades. The miniSOG-CLEA is a recyclable heterogeneous photocatalyst: it retains activity over multiple reuse cycles and activity loss is due to photobleaching rather than leaching (the FMN cofactor remains entrapped), and stored samples remain active. Unlike conventional inorganic photocatalysts (*e.g.*, TiO_2), here a single bioderived solid enables two biocatalysis-compatible modes under visible light and in water: (i) at neutral pH it delivers a controlled H_2O_2 feed for oxidative enzymes, and (ii) under alkaline conditions it photo-oxidizes TEOA to glycolaldehyde, which drives NADH regeneration, a functionality uncommon for inorganic materials. While its ability to produce a relatively small amount of the desired species (H_2O_2, NADH equivalents), remains a barrier, this study opens the road for further improvements, for instance by genetic engineering (more photostable fluorescent proteins *etc*), or more advanced reaction set ups. Continuous flow would be a good candidate for such an endeavour, as preparative-scale CLEAs have already been produced for lipases, showing that the precipitation/cross-link cycle scales with the same equipment used for routine enzyme processing.[68] The resulting mechanically robust aggregates can be pumped as slurries or packed into transparent packed-bed columns, and illuminated.[69] Continuous-flow reactors have operated smoothly with such CLEA formulations at litre-per-hour throughputs, demonstrating seamless integration of CLEAs into modern flow-chemistry platforms.[70]

Author contributions

F. P. and E. B. conceptualized the idea. F. P. supervised the project and acquired funding. E. B. performed the experiments and wrote the initial draft. Both authors discussed the results and reviewed the manuscript.

Conflicts of interest

There are no conflicts to declare.

Data availability

The data supporting this article have been included as part of the SI. See DOI: **https://doi.org/10.1039/d5ma00861a**.

Acknowledgements

This project was supported by the SNSF (200021_232199, F.P). We thank Prof. Frank Hollmann for providing the lyophilised AaeUPO enzyme and for useful scientific discussions.

Notes and references

1 J. Chen, J. Cen, X. Xu and X. Li, *Catal. Sci. Technol.*, 2016, **6**, 349–362.
2 A. Savateev and M. Antonietti, *ACS Catal.*, 2018, **8**, 9790–9808.
3 D. Friedmann, A. Hakki, H. Kim, W. Choi and D. Bahnemann, *Green Chem.*, 2016, **18**, 5391–5411.
4 A. Fujishima, T. N. Rao and D. A. Tryk, *J. Photochem. Photobiol., C*, 2000, **1**, 1–21.
5 S. Cao, J. Low, J. Yu and M. Jaroniec, *Adv. Mater.*, 2015, **27**, 2150–2176.
6 D. Taylor, S. J. Dalgarno, Z. Xu and F. Vilela, *Chem. Soc. Rev.*, 2020, **49**, 3981–4042.
7 A. Bavykina, N. Kolobov, I. S. Khan, J. A. Bau, A. Ramirez and J. Gascon, *Chem. Rev.*, 2020, **120**, 8468–8535.
8 X. Wang, K. Maeda, A. Thomas, K. Takanabe, G. Xin, J. M. Carlsson, K. Domen and M. Antonietti, *Nat. Mater.*, 2009, **8**, 76–80.

9 M. J. Alonso-Navarro, J. Barrio, S. Royuela, N. Karjule, M. M. Ramos, J. I. Martínez, M. Shalom and J. L. Segura, *RSC Adv.*, 2021, **11**, 2701–2705.
10 T. Zhang, C. Si, K. Guo, X. Liu, Q. Liu, J. Fu and Q. Han, *Inorg. Chem.*, 2022, **61**, 20657–20665.
11 V. Srivastava, P. K. Singh, A. Srivastava and P. P. Singh, *RSC Adv.*, 2021, **11**, 14251–14259.
12 R. Cibulka and M. W. Fraaije, *Flavin-Based Catalysis*, John Wiley & Sons, Ltd, 2021, pp. 97–124.
13 T. Pavlovska, D. Král Lesný, E. Svobodová, I. Hoskovcová, N. Archipowa, R. J. Kutta and R. Cibulka, *Chem. – Eur. J.*, 2022, **28**, e202200768.
14 P. Dongare, I. MacKenzie, D. Wang, D. A. Nicewicz and T. J. Meyer, *Proc. Natl. Acad. Sci. U. S. A.*, 2017, **114**, 9279–9283.
15 V. Mojr, E. Svobodová, K. Straková, T. Neveselý, J. Chudoba, H. Dvořáková and R. Cibulka, *Chem. Commun.*, 2015, **51**, 12036–12039.
16 O. Cabezuelo, R. Martinez-Haya, N. Montes, F. Bosca and M. L. Marin, *Appl. Catal., B*, 2021, **298**, 120497.
17 P. Tang, B. Ji and G. Sun, *J. Hazard. Mater.*, 2022, **435**, 128982.
18 S. F. Castillo Pacheco, M. J. Moran, J. I. Santos, L. Salassa and F. López-Gallego, *ChemCatChem*, 2023, **15**, e202300140.
19 F. Parmeggiani, E. Brenna, D. Colombo, F. G. Gatti, F. Tentori and D. Tessaro, *ChemBioChem*, 2022, **23**, e202100445.
20 K. Stott, K. Saito, D. J. Thiele and V. Massey, *J. Biol. Chem.*, 1993, **268**, 6097–6106.
21 X. Shu, V. Lev-Ram, T. J. Deerinck, Y. Qi, E. B. Ramko, M. W. Davidson, Y. Jin, M. H. Ellisman and R. Y. Tsien, *PLoS Biol.*, 2011, **9**, e1001041.
22 O. Azpitarte, A. Zudaire, J. Uranga, X. Lopez, L. Salassa, E. Formoso and E. Rezabal, *ChemPhysChem*, 2023, **24**, e202300091.
23 J. Gurruchaga-Pereda, V. Martínez-Martínez, E. Formoso, O. Azpitarte, E. Rezabal, X. Lopez, A. L. Cortajarena and L. Salassa, *J. Phys. Chem. Lett.*, 2021, **12**, 4504–4508.
24 E. A. Souslova, K. E. Mironova and S. M. Deyev, *J. Biophotonics*, 2017, **10**, 338–352.
25 J. Torra, C. Lafaye, L. Signor, S. Aumonier, C. Flors, X. Shu, S. Nonell, G. Gotthard and A. Royant, *Sci. Rep.*, 2019, **9**, 2428.
26 J. Chen, R. Prinsloo and X. Ni, *Technologies*, 2024, **12**, 29.
27 K. Ohkubo, T. Nanjo and S. Fukuzumi, *Bull. Chem. Soc. Jpn.*, 2006, **79**, 1489–1500.
28 J. Al-Nu'airat, I. Oluwoye, N. Zeinali, M. Altarawneh and B. Z. Dlugogorski, *Chem. Rec.*, 2021, **21**, 315–342.
29 S. Mondal, R. B. Jethwa, B. Pant, R. Hauschild and S. A. Freunberger, *Faraday Discuss.*, 2024, **248**, 175–189.
30 J. A. Navio, J. Fuentes Mota, M. A. Pradera Adrian and M. Garcia Gomez, *J. Photochem. Photobiol., A*, 1990, **52**, 91–95.
31 R. Ruiz-González, A. L. Cortajarena, S. H. Mejias, M. Agut, S. Nonell and C. Flors, *J. Am. Chem. Soc.*, 2013, **135**, 9564–9567.
32 D. V. Yuzhakova, M. V. Shirmanova, V. V. Klimenko, M. M. Lukina, A. I. Gavrina, A. D. Komarova, D. A. Gorbachev, N. V. Sapogova, K. A. Lukyanov and V. A. Kamensky, *Biochim. Biophys. Acta, Gen. Subj.*, 2021, **1865**, 129978.
33 F. Hilgers, N. L. Bitzenhofer, Y. Ackermann, A. Burmeister, A. Grünberger, K. E. Jaeger and T. Drepper, *Int. J. Mol. Sci.*, 2019, **20**, 4608.
34 A. Karich, K. Scheibner, R. Ullrich and M. Hofrichter, *J. Mol. Catal. B: Enzym.*, 2016, **134**, 238–246.
35 E. Broumidis and F. Paradisi, *Angew. Chem., Int. Ed.*, 2024, **63**, e202401912.
36 P. Püllmann, D. Homann, T. A. Karl, B. König and M. J. Weissenborn, *Angew. Chem., Int. Ed.*, 2023, **62**, e202307897.
37 S. Willot, E. Fernández-Fueyo, F. Tieves, M. Pesic, M. Alcalde, I. W. C. E. Arends, C. B. Park and F. Hollmann, *ACS Catal.*, 2019, **9**, 890–894.
38 P. De Santis, D. Wegstein, B. O. Burek, J. Patzsch, M. Alcalde, W. Kroutil, J. Z. Bloh and S. Kara, *ChemSusChem*, 2023, **16**, e202300613.
39 D. J. Mogensen, M. Etzerodt and P. R. Ogilby, *J. Photochem. Photobiol., A*, 2022, **429**, 113894.
40 M. Westberg, L. Holmegaard, F. M. Pimenta, M. Etzerodt and P. R. Ogilby, *J. Am. Chem. Soc.*, 2015, **137**, 1632–1642.
41 S. Talekar, A. Joshi, G. Joshi, P. Kamat, R. Haripurkar and S. Kambale, *RSC Adv.*, 2013, **3**, 12485–12511.
42 C. Blanco-Llamero, P. García-García and F. J. Señoráns, *Front. Bioeng. Biotechnol.*, 2021, **9**, DOI: **10.3389/fbioe.2021.794672**.
43 K. C. Duong-Ly and S. B. Gabelli, in *Methods in Enzymology*, ed. J. Lorsch, Academic Press, 2014, vol. 541, pp. 85–94.
44 O. Savateev and Y. Zou, *ChemistryOpen*, 2022, **11**, e202200095.
45 E. D. Getzoff, D. E. Cabelli, C. L. Fisher, H. E. Parge, M. S. Viezzoli, L. Banci and R. A. Hallewell, *Nature*, 1992, **358**, 347–351.
46 E. Churakova, M. Kluge, R. Ullrich, I. Arends, M. Hofrichter and F. Hollmann, *Angew. Chem., Int. Ed.*, 2011, **50**, 10716–10719.
47 M. E. Barnett, T. M. Baran, T. H. Foster and A. P. Wojtovich, *Free Radical Biol. Med.*, 2018, **116**, 134–140.
48 F. M. Pimenta, R. L. Jensen, T. Breitenbach, M. Etzerodt and P. R. Ogilby, *Photochem. Photobiol.*, 2013, **89**, 1116–1126.
49 C. S. Sampaio, J. A. F. Angelotti, R. Fernandez-Lafuente and D. B. Hirata, *Int. J. Biol. Macromol.*, 2022, **215**, 434–449.
50 R. A. Sheldon, *Biochem. Soc. Trans.*, 2007, **35**, 1583–1587.
51 A. Borham, M. Bkhit, J. Wang and X. Qian, *Environ. Technol. Innovation*, 2025, **38**, 104143.
52 J. S. Cobb, V. Zai-Rose, J. J. Correia and A. V. Janorkar, *ACS Omega*, 2020, **5**, 8403–8413.
53 M. S. M. Razib, R. N. Z. R. A. Rahman, F. M. Shariff and M. S. M. Ali, *Catalysts*, 2020, **10**, 55.
54 S. A. Chaudhari and R. S. Singhal, *Int. J. Biol. Macromol.*, 2017, **98**, 610–621.
55 S. S. Tükel, F. Hürrem, D. Yildirim and Ö. Alptekin, *J. Mol. Catal. B: Enzym.*, 2013, **97**, 252–257.
56 R. Schoevaart, M. W. Wolbers, M. Golubovic, M. Ottens, A. P. G. Kieboom, F. van Rantwijk, L. A. M. van der Wielen and R. A. Sheldon, *Biotechnol. Bioeng.*, 2004, **87**, 754–762.

57 M. Sadauskas, R. Statkevičiūtė, J. Vaitekūnas, V. Petkevičius, V. Časaitė, R. Gasparavičiūtė and R. Meškys, *Dyes Pigm.*, 2020, **173**, 107882.
58 R. Ullrich, M. Poraj-Kobielska, O. M. Herold-Majumdar, J. Vind and M. Hofrichter, *Catalysts*, 2021, **11**, 1495.
59 J. Ribes, P. Cossard, K. Al Yaman, I. Bestel and E. Badarau, *RSC Adv.*, 2023, **13**, 2355–2364.
60 K. Bachosz, J. Zdarta, M. Bilal, A. S. Meyer and T. Jesionowski, *Sci. Total Environ.*, 2023, **868**, 161630.
61 K. Kinastowska, J. Liu, J. M. Tobin, Y. Rakovich, F. Vilela, Z. Xu, W. Bartkowiak and M. Grzelczak, *Appl. Catal., B*, 2019, **243**, 686–692.
62 Y. Li, D. Si, W. Shang, J. Wang, J. Guo, N. Zhang, C. Hao and Y. Shi, *New J. Chem.*, 2022, **46**, 6360–6365.
63 G. Yao, K. Liu, S. Wang, H. Huo and S. Wang, *J. Chem. Technol. Biotechnol.*, 2021, **96**, 1049–1056.
64 A. L. Ahmad, E. M. Low and S. R. A. Shukor, *J. Mol. Catal. B: Enzym.*, 2013, **88**, 26–31.
65 I. E. Touahar, L. Haroune, S. Ba, J.-P. Bellenger and H. Cabana, *Sci. Total Environ.*, 2014, **481**, 90–99.
66 L. T. Nguyen and K.-L. Yang, *Enzyme Microb. Technol.*, 2017, **100**, 52–59.
67 D. Yang, Y. Zhang, S. Zhang, Y. Cheng, Y. Wu, Z. Cai, X. Wang, J. Shi and Z. Jiang, *ACS Catal.*, 2019, **9**, 11492–11501.
68 R. Fernández-Penas, C. Verdugo-Escamilla, S. Martínez-Rodríguez and J. A. Gavira, *Cryst. Growth Des.*, 2021, **21**, 1698–1707.
69 S. Simić, M. Jakštaitė, W. T. S. Huck, C. K. Winkler and W. Kroutil, *ACS Catal.*, 2022, **12**, 14040–14049.
70 C. L. Fernández Regueiro, D. Roura Padrosa and F. Paradisi, *C. R. Chim*, 2025, **28**, 349–359.